Technical Paper

ISSN 1997-1400 Int. J. Pavement Res. Technol. 4(2):89-96
Copyright @ Chinese Society of Pavement Engineering

Measurement and Analysis of Early-age Strain and Stress in Continuously Reinforced Concrete Pavement

Hong-liang Zhang[1+] and Yan-hui Wang[2]

Abstract: The measured strains in the continuously reinforced concrete pavement (CRCP) cannot simply be used to calculate the concrete stresses by multiplying the elastic modulus of concrete, because the measured strains include both the stress dependent and independent strains. The setting temperature of concrete and the measured strain at this temperature should be used to calculate the temperature difference and the strain increment. The early-age strains in the concrete and steel of CRCP were measured in this paper. The measured concrete strains include the total strain, the stress independent strain and the initial strain at setting temperature. These measured values can be used not only to accurately calculate the stresses in concrete and steel but also to determine the accurate boundary conditions in the numerical modeling of CRCP subject to environmental loading. On the boundary conditions used in analysis of the early-age CRCP under environmental loading, epoxy coated steel is not completely bonded with concrete. Additionally, the perfectly free or restrained boundary condition across cracking is not true, and the longitudinal steel strains across cracking will help develop the proper boundary condition across cracking. The calculated stress was verified from the comparison between the calculated stress at the instant of cracking and the measured tensile strength.

Key words: Boundary condition, CRCP, Environmental loading, Early-age, Strain.

Introduction

In recent years, great progress has been made regarding research on continuously reinforced concrete pavement (CRCP). In the 1993 AASHTO guide, the performance criteria of CRCP include crack spacing, crack width, and the tensile stress in the steel [1]. In NCHRP 1-37A [2], the performance criteria consist of punch-out development and smoothness, as well as crack width if deemed necessary. Many studies have focused on the following fields of CRCP: the effects of design and construction factors on CRCP performance [2-6], the numerical modeling of CRCP under traffic and environmental loading (or loads) [7-11], construction technique [12-14], and the prediction of crack progression, punch-outs, etc. [2, 12].

To a large extent, the performance of CRCP depends on its early-age behavior. Thus, some researchers have studied the early-age behavior of CRCP [5, 6, 13, 15, 16], but because testing in actual field CRCP poses difficulties such as proper scheduling with contractors, installing testing equipment, and setting up traffic control for detailed field condition survey after the pavement is open to traffic, a majority of studies have been conducted in the laboratory. Simulating CRCP in the laboratory has limitations in understanding true CRCP behaviors. These limitations are partly due to the difficulty in setting boundary conditions of CRCP in small scale and generating actual environmental and traffic loadings. To understand actual behaviors of CRCP, these limitations make it necessary to conduct testing in actual field CRCP.

The field study on the early-age microscopic behavior, in terms of strains and stresses, of CRCP is rare. Nam *et al*. [15] and Kim *et al*. [16] investigated the early-age behavior of CRCP in terms of concrete strains and stresses from environmental loading. However, they did not measure the steel strain or concrete setting temperature. Kohler *et al*. [13] extensively investigated the early-age behavior of ten CRCP test sections with extended lives at the Advanced Transportation, Research, and Engineering Laboratory (ATREL), but they did not measure the stress independent strain of concrete. The measured strains in the actual CRCP cannot simply be used to calculate the concrete stresses by multiplying the elastic modulus of concrete because the measured strains include both the stress dependent and independent strains. The setting temperature of concrete and the measured strain at this temperature should be used to calculate the total temperature difference and strain increment of the concrete. Both the measurements of the stress independent strain and the setting temperature are very important to accurately calculate the stress in concrete. On the other hand, the measurement of steel strain can help determine the accurate boundary condition for the numerical model of CRCP subjected to environmental loads. Due to the deficiency in field data, most of the theoretical research on CRCP has been conducted with simplified boundary assumptions such as the perfectly restrained condition. The simplified boundary conditions need to be verified or corrected.

In addition, there are a lot of differences in climate, material, traffic, structure, design level, and construction techniques among the CRC pavements of different countries, which have great effects on the early-age behavior of CRCP. In China, the extensive measurement of the early-age strain and stress in CRCP has not been conducted yet.

In order to understand the true early-age behavior of CRCP in

[1] Associate Professor, Key Laboratory for Special Area Highway Engineering of Ministry of Education of China, Highway College of Chang'an University, P. O. Box 329, Xi'an, Shaanxi, 710064, PR China.

[2] Key Laboratory for Special Area Highway Engineering of Ministry of Education of China, Highway College of Chang'an University, Xi'an, Shaanxi, 710064, PR China.

[+] Corresponding Author: E-mail L29@GL.CHD.EDU.CN

Note: Submitted January 7, 2010; Revised April 28, 2010; Accepted May 12, 2010

Table 1. CRCP Test Sections.

Section	Starting and Ending	Pavement Structure	Crack Control Program
1	K158+150 - K158+350	30 cm CRC + 4 cm AC + 20 cm CTB + 20 cm GA	K158+150 - K158+180: Induced Crack at Spacing of 1 m K158+180 - K158+210: Induced Crack at Spacing of 1.5 m K158+210 - K158+240: Induced Crack at Spacing of 2 m K158+240 - K158+350: Passive Crack
2	K158+400 - K158+600	30 cm CRC + 10 cm ATB + Seal Coat + 20 cm GA	K158+400 - K158+430: Induced Crack at Spacing of 2 m K158+430 - K158+460: Induced Crack Spacing of 2.5 m K158+460 - K158+490: Induced Crack at Spacing of 3 m K158+490 - K158+600: Passive Crack

Note: AC means asphalt concrete; CTB means cement treated base and is open graded; GA means graded aggregate; and ATB means asphalt treated base.

Table 2. Concrete Mixture Design (kg/m^3).

Cement	Water	Coarse Aggregate	Fine Aggregate	Admixture
363	143	1156	708	5.08

China and to determine the accurate boundary conditions in the numerical modeling of CRCP subjected to environmental loads, two CRCP test sections were built in Yanwei Expressway (fromYantai city to Weihai city). The strains in the concrete and steel of CRCP were measured. The measured strains in concrete included the total strain, the stress independent stain and the initial strain at setting temperature. Based on measurement results, the boundary conditions in the numerical modeling of CRCP subjected to environmental loads were discussed also.

Design of Test Sections

Two test sections, as listed in Table 1, were constructed in October 2008. In both of these test sections, the percentage of longitudinal steel is 0.7%, and its depth from the surface of CRCP is 9 cm. The transverse steel is perpendicular to the longitudinal steel, both the transverse and longitudinal steels are epoxy coated, the shoulders are tied, and lug anchors are used at terminal joints.

CRCP has traditionally been allowed to crack naturally. This type of passive crack control has resulted in non-uniform crack spacing, which has led to premature distress development. When active crack control was used on CRCP, more uniform, straighter, and early-age developing transverse cracks resulted, which increased the expected service life of CRCP [14]. Thus, both passive and active crack control types were used in these two CRCP test sections. A Soff-cut@ saw was used to cut a 3.8 cm notch in the CRCP surface. The induced crack spacing ranged from 1 m to 5 m. The early entry saw-cutting occurred approximately four hours after concrete placement. The detailed crack control program is listed in Table 1.

The target flexural strength for the concrete design is approximately 5.0 MPa at 28-days of age, and the design w/c ratio and design air content are 0.40 and 5.0%, respectively [17]. The coarse aggregate is made from limestone. The mix design is detailed in Table 2. Both air entraining and water reducing admixture are used.

Concrete Strain and Stress Analysis Method

The total strain of concrete consists of stress dependent strain and stress independent strain. The stress dependent strain ε_i^{σ}, which is produced by stresses in the concrete, is the sum of the elastic strain ε_i^{e} and the creep strain ε_i^{c}. On the other hand, the stress independent strain ε_i^{0}, which is not related to stress, is the sum of the thermal strain ε_i^{th} and the shrinkage strain ε_i^{sh}. Therefore, the total strain increment during time step Δt_r is as follows [18].

$$\Delta\varepsilon_i^{T} = \Delta\varepsilon_i^{\sigma} + \Delta\varepsilon_i^{0} = \Delta\varepsilon_i^{e} + \Delta\varepsilon_i^{c} + \Delta\varepsilon_i^{th} + \Delta\varepsilon_i^{sh} \quad (1)$$

where $\Delta\varepsilon_i^{T}$ is the total strain increment; $\Delta\varepsilon_i^{\sigma}$ is the stress dependent strain increment; $\Delta\varepsilon_i^{0}$ is the stress independent strain increment; $\Delta\varepsilon_i^{e}$ is the elastic strain increment; $\Delta\varepsilon_i^{c}$ is the creep strain increment; $\Delta\varepsilon_i^{th}$ is the thermal strain increment; and $\Delta\varepsilon_i^{sh}$ is the shrinkage strain increment.

The stress σ_i can be calculated by multiplying the stress dependent strain increment, which is equal to the difference between the total strain increment and the stress independent strain increment, by the elastic modulus E_i.

$$\sigma_i = E\times\Delta\varepsilon_i^{\sigma} = E\times(\Delta\varepsilon_i^{T} - \Delta\varepsilon_i^{0}) \quad (2)$$

Since the initial strain at the setting temperature of the total strain is equal to that of the independent strain, it can be surmised from Eq. (2) that:

$$\sigma_i = E\times(\varepsilon_i^{T} - \varepsilon_i^{0}) = E\times\varepsilon_i^{\sigma} \quad (3)$$

Instrumentation of Test Sections

A variety of sensors were installed in these two sections, and the instrumentation and test results were similar. Therefore, only the instrumentation and test results in section 2 are provided in this paper.

The set of instruments only includes static system. The static system refers to all the sensors intended to record the pavement responses induced by static traffic loading. The system also collects data related to the early-age responses due to hydration and shrinkage of the concrete combined with the local environmental conditions during construction. The static system is composed strain gauges in the concrete, strain gauges on the reinforcement bars,

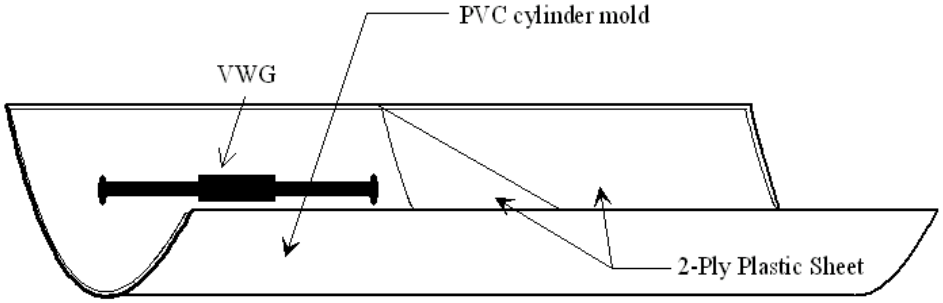

Fig.1. Stress Independent Strain Measurement Devices.

thermocouples, and stress-independent strain measurement devices. The static strain gauges are Vibrating Wire Gauges (VWGs).

A conceptual diagram of the stress independent strain measurement device is shown in Fig. 1 [15]. VWGs were installed inside a half cylinder to measure stress independent strains. A double layer of plastic sheets were fitted inside the mold to minimize the friction between the inside of the mold and the concrete. Similar two-ply plastic sheets were used at both ends of the mold as membranes to ensure the separation of the concrete inside and outside of the mold when the tensile stress started developing in the concrete. Two-ply plastic sheets were also used at the top of the mold to minimize the friction between the concretes inside and outside of the mold. The stress independent strain measurement device is placed directly in the newly paved concrete.

The locations of concrete strain gauges, stress independent strain measurement devices, and thermocouples are shown in Fig. 2 (a). The locations of reinforcement strain gauges are shown in Fig. 2 (b).

To place sensors at the desired locations, a number of pairs of wooden dowels were driven into the sub-base, and the sensors were tied to the dowels. To ensure transverse cracking at the location where gauges were installed, a Soff-cut@ saw was used to cut a 3.8 cm notch in the CRCP surface. The static concrete strain gauges across cracks at the locations of a and c were functional for strain measurements prior to the crack formation, but afterwards, they are functional for crack width measurement. They were positioned at 5 different depths. If at one location there are several sensors at different depths, they are numbered as (1), (2), and (3) etc. Concrete strain gauges were installed at approximately 190 cm from the outside lane edge [15].

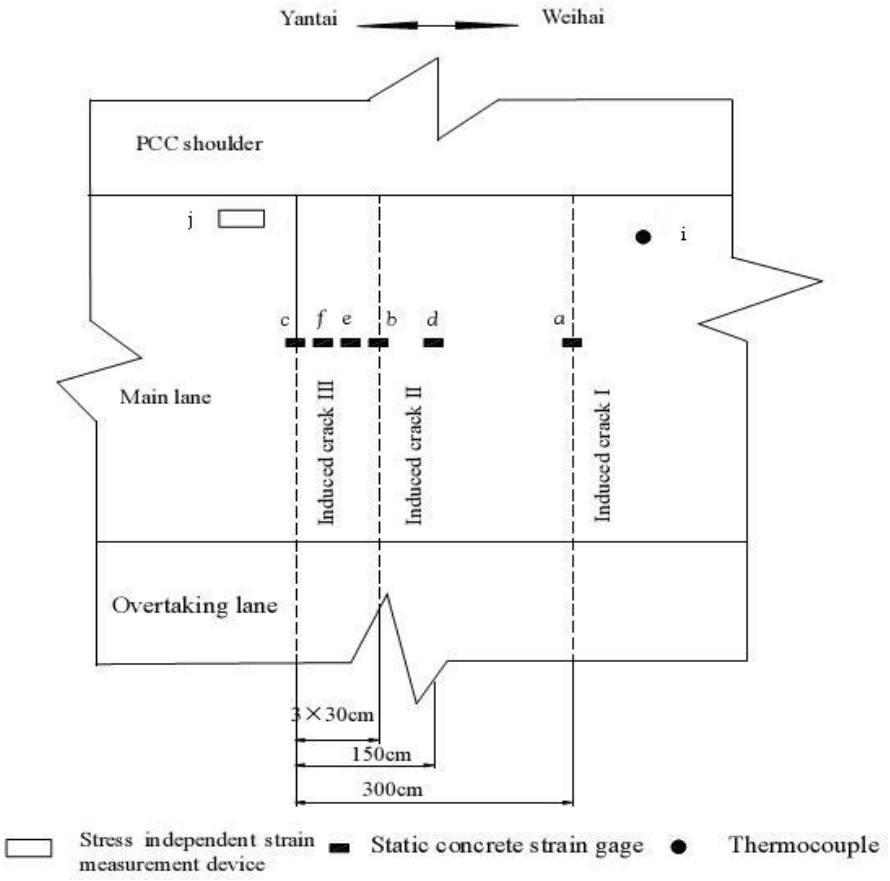

Fig. 2 (a). Locations of Concrete Strain Gauges, Stress Independent Strain Measurement Device and Thermocouples.

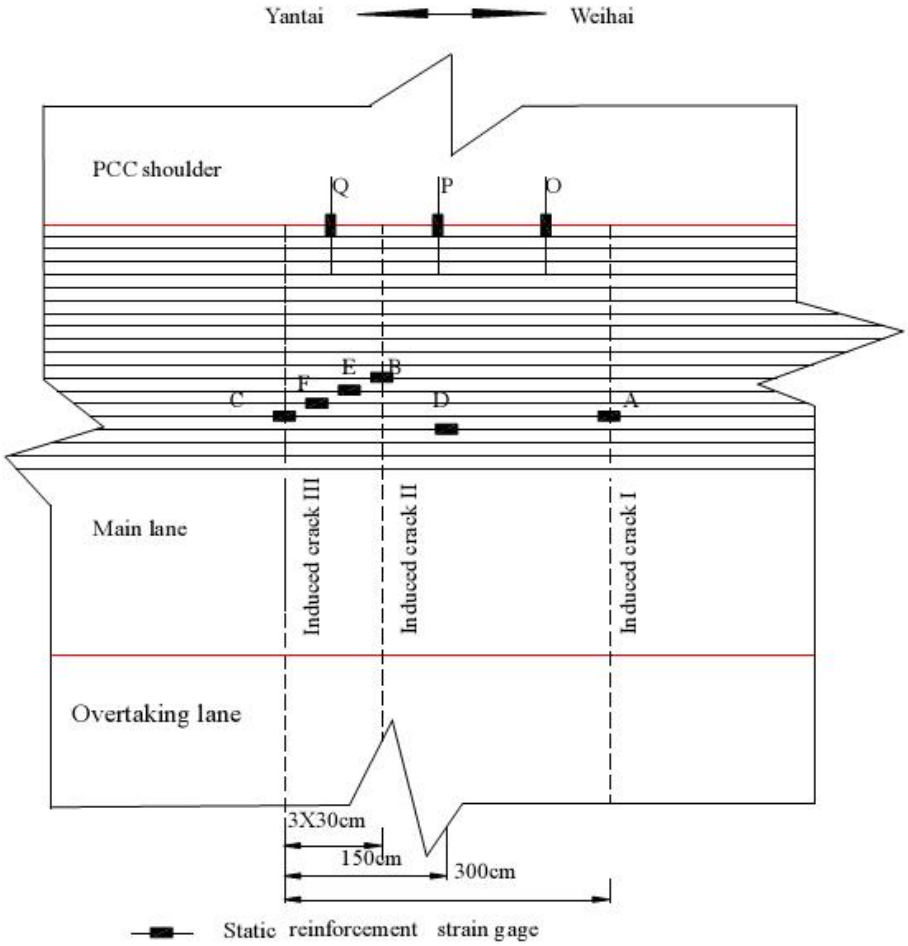

Fig. 2 (b). Locations of Reinforcement Strain Gauges

The number and depth of the sensors at each location are listed in detail in Table 3. The transverse spacing of the longitudinal reinforcements is 12 cm and the longitudinal reinforcements are numbered as 1, 2, 3, etc. in the direction of pavement edge to pavement middle. The distance between the first longitudinal reinforcement and the slab edge is 10 cm. Static reinforcement strain gauges A, B, C, D, E and F were mounted on the 15^{th}, 12^{th}, 15^{th}, 16^{th}, 13^{th} and 14^{th} longitudinal reinforcement bars, respectively. Static reinforcement strain gauges O, P and Q were mounted on the tie bars.

In order to capture the climatological data in the analysis, a weather station was installed at the site. The weather station recorded air temperature, humidity, wind speed, wind direction, and solar radiation.

Concrete Strength and Modulus

Concrete specimens were prepared in the test sites. These specimens were moist cured and tested at 3, 7, 14, 28 and 90 days of age. Table 4 lists the measured concrete compressive, splitting and flexural strengths, as well as compressive and flexural moduli.

Early-age Strains

Concrete Stress Independent Strain

The coefficient of thermal expansion (*COTE*) of concrete was determined to be $5.5\times10^{-6}/℃$ in the laboratory. Figs. 3 and 4 show the plots of the measured concrete temperatures and stress independent strains vs. time data in which negative strain is compressive and positive strain extends. Based on the previous *COTE* test results, the in situ drying shrinkage strain can be obtained as the difference between the stress independent strain and the thermal strain (Eq. (4)). The drying shrinkage strains are also shown in Figs. 3 and 4. From these two figures, it can be seen that the stress independent strain and the drying shrinkage strain are related to the depth in the slab.

$$\Delta\varepsilon_i^{sh} = \Delta\varepsilon_i^{\,0} - \Delta\varepsilon_i^{\,sh} = \Delta\varepsilon_i^{\,0} - \Delta T \times COTE \tag{4}$$

Total Strain of Concrete and Steel

The following text discusses (1) the concrete strain variation through depth before cracking, (2) the concrete setting temperature, and (3) the longitudinal steel strain.

Concrete Strain Variation through Depth before Cracking

Table 3. Number and Depth of Sensor at Each Location.

Sensors		Depth from Concrete Surface (cm)	Layer Located
Static Concrete Strain Gauges	*a*(1)	7.0	Concrete Slab
	a(2)	14.0	Concrete Slab
	a(3)	26.5	Concrete Slab
	a(4)	34.0	AC Separating Layer
	a(5)	54.0	CTB Base
	b	7.0	Concrete Slab
	c(1)	7.0	Concrete Slab
	c(2)	13.2	Concrete Slab
	c(3)	26.0	Concrete Slab
	c(4)	34.0	AC Separating Layer
	c(5)	54.0	CTB Base
	d	2.5	Concrete Slab
	e	2.5	Concrete Slab
	f	2.5	Concrete Slab
Thermocouples	i(1)	2.5	Concrete Slab
	i(2)	10.0	Concrete Slab
	i(3)	16.0	Concrete Slab
	i(4)	20.7	Concrete Slab
	i(5)	27.5	Concrete Slab
	i(6)	32.0	AC Separating Layer
	i(7)	42.0	CTB Base
Stress Independent Strain Measurement Device	j(1)	2.5	Concrete Slab
	j(2)	10.0	Concrete Slab

Table 4. Materials and Properties Test Results.

Age (d)	Compressive Strength (MPa)	Flexural Strength (MPa)	Splitting Strength (MPa)	Compressive Modulus (GPa)	Flexural Modulus (GPa)
3	12.9	2.5	1.0	13.8	23.8
7	37.1	4.1	1.6	22.6	29.6
14	42.2	4.8	2.4	29.2	32.1
28	45.0	5.3	3.1	36.1	34.2
90	48.2	5.5	3.6	37.8	38.1

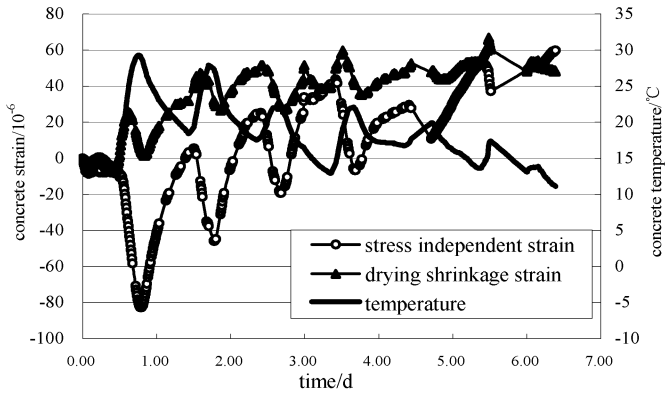

Fig. 3. Time Histories of Stress Independent Strain and Drying Shrinkage Strain and Temperature at Location j(1).

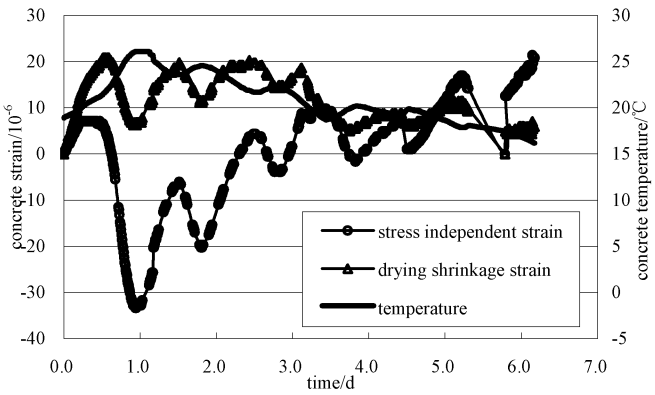

Fig. 4. Time Histories of Stress Independent Strain and Drying Shrinkage Strain and Temperature at Location j(2)

Fig. 5 shows the variations of concrete total strains before the first transverse crack occurred in Crack III, measured using VWGs at three different depths. Total strain variations are not directly proportional to the concrete temperature variations because of the restraint of boundary conditions of the CRCP structure. The total strain is the sum of the stress independent strain and the stress dependent strain, and the stress independent strain is usually proportional to the environmental load. It can be concluded that the

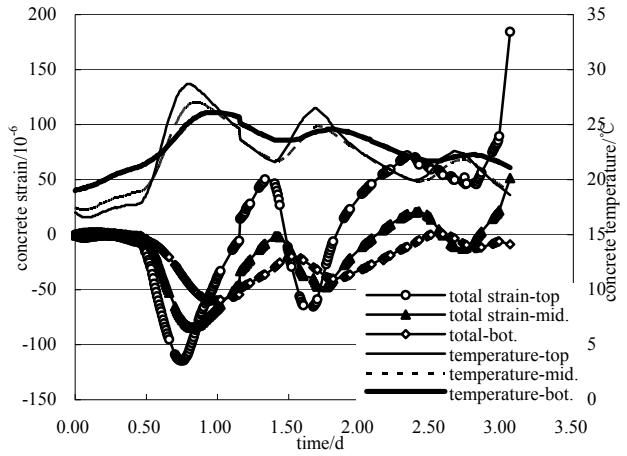

Fig. 5. Concrete Total Strains and Temperatures at Induced Crack III before Cracking.

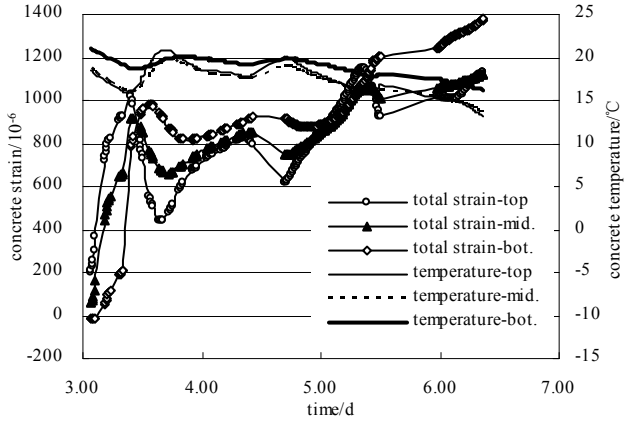

Fig. 6. Concrete Total Strains and Temperatures at Induced Crack III after Cracking.

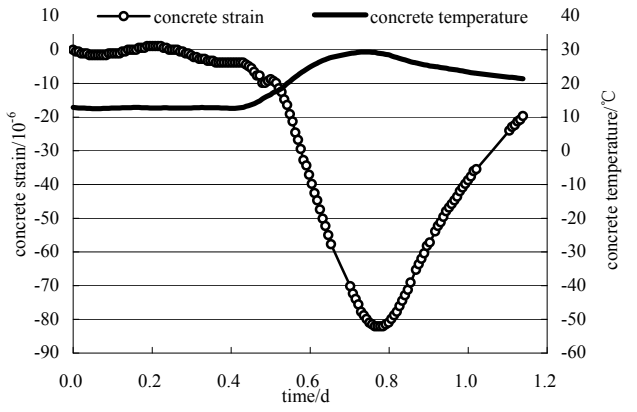

Fig. 7. Variations of Concrete Strain and Temperature in Concrete after Concrete Placement at Location j(1).

stress dependent strain is not directly proportional to the concrete temperature variations and is governed by the structural boundary conditions. Most of the research on CRCP has been conducted with simplified boundary assumptions, such as the perfectly restrained condition. If the perfectly restrained condition is true, the total strain should not change with time before cracking. However, the total strain at the crack induced area varies with time before cracking.

Table 5. Setting Temperatures and Initial Strains.

Section	Location	Setting temperature(℃)	Initial strain (10^{-6})
1	j(1)	18.9	-11.0
1	j(2)	25.4	-2.7
2	j(1)	18.5	-13.0
2	j(2)	21.7	3.0

The induced cracks occurred about three days after placement of the concrete. The measured data are shown in Fig. 6. After cracking, the measured total strain multiplied by the VWG length is considered the crack width.

Concrete Setting Temperature

Setting temperature is reported to have substantial effects on crack widths. To determine the setting temperature, a method devised by Glisic *et al* was applied [19]. The method is based on the fact that VWGs and temperatures move in the same direction while concrete is plastic and does not exert restraint on VWGs. It also stipulates that once concrete starts setting and the concrete and VWG start moving together, strains in VWG and temperatures move in opposite directions. Fig. 7 shows the variations in temperatures and strains in concrete after concrete placement at location *j*(1). The figure illustrates that the temperature and concrete strain move in the same direction until about 12 hours after concrete placement, at which point the temperature and concrete strain start moving in opposite directions. The temperature and concrete strain at this point are defined as setting temperature and initial strain, respectively. It can be discerned from Fig. 7 that the setting temperature is 18.5℃ and the initial strain is -13.0 $\times 10^{-6}$ at location *j*(1). Similarly, the setting temperature and the initial strain at j(2) in section 2 and at j(1) and j(2) in section 1 can be determined. The measured setting temperatures and the initial strains are listed in Table 5. Section 1 and section 2 were cast on different days and j(1) and j(2) were different in depth. So from Table 5, it can be seen that the setting temperature and initial strain are the functions of depth and cast time. The initial strain should be subtracted from the subsequent strain readings and the resultant values are strain increments.

Longitudinal Steel Strain

The longitudinal steel strain variations are shown from Figs. 8 to 11. The longitudinal steel strains increase suddenly at cracking. At this time, the stresses in concrete are relieved at the crack, and the relieved stresses are transferred to the steel. The longitudinal steel strain across cracking will help develop proper boundary conditions across cracking for a more accurate analysis of CRCP under environmental loads.

A comparison of the concrete strain and steel strain at approximately the same position shows that these two strains are not equal to each other. For example, the concrete strains at induced

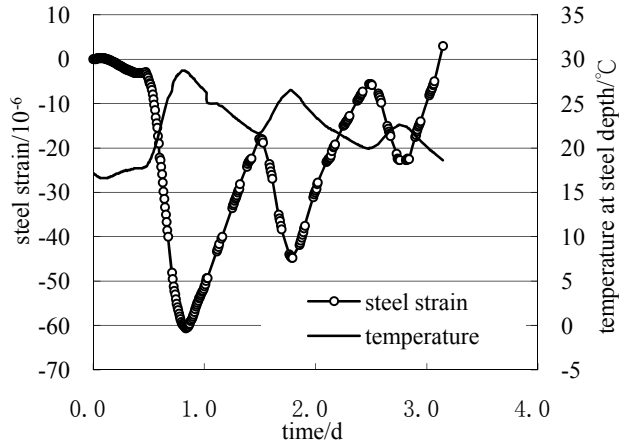

Fig. 8. Longitudinal Steel Strain and Temperature Variations at Induced Crack I before Cracking.

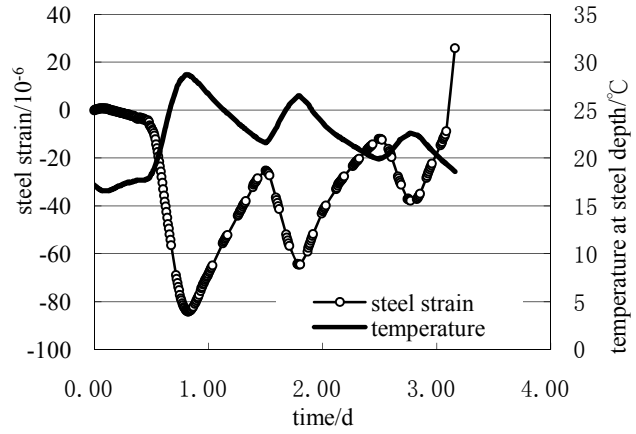

Fig. 9. Longitudinal Steel Strain and Temperature Variations at Induced Crack III before Cracking.

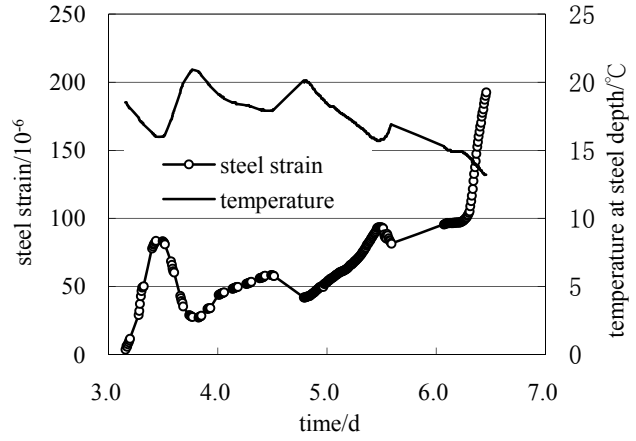

Fig. 10. Longitudinal Steel Strain and Temperature Variations at Induced Crack I after Cracking.

Crack III measured in November 2008 are 184 $\times 10^{-6}$ and 51 $\times 10^{-6}$ at the depths of 7.0 cm and 13.2 cm, respectively. The concrete strain at the depth of 9 cm lies within the range of 51×10^{-6} to 184×10^{-6}.

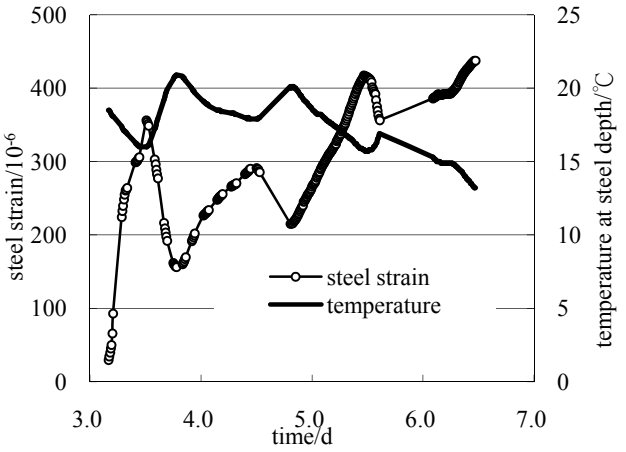

Fig. 11. Longitudinal Steel Strain and Temperature Variations at Induced Crack III after Cracking.

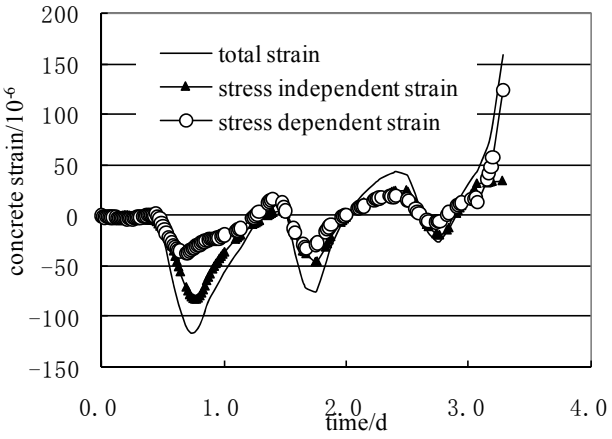

Fig. 12. Concrete Strain Variations at Location a(1).

However, the steel strain measured at the depth of 9 cm at induced Crack III was 26×10^{-6}. So it is unreasonable to assume that the steel is completely bonded with the concrete in the analysis of the early-age performance of CRCP.

Concrete Stress Calculation

Fig. 12 shows the measured total strain, measured stress independent strain, and calculated stress dependent strain in the concrete at location a(1). The crack occurred at about 3 days of age, and the stress dependent strain is about 124×10^{-6}. From Table 4, it can be discerned that the elastic modulus and flexural strength of concrete after 3 days are 13.8 GPa and 2.5 MPa, respectively. According to reference [2], the tensile strength of concrete is about 0.6~0.7 of its flexural strength. Thus, the tensile strength of concrete at day 3 lies within the range. According to Eq. (3), the stress at cracking can be determined as 1.71 MPa, which is very close to the tensile strength at day 3. Therefore, the concrete strain concrete stress analysis method for CRCP explained in this paper has been verified.

Summary and Conclusions

Two CRCP test sections were built in the Yanwei Expressway in China. The early-age strains in concrete and steel were measured, and the stress in concrete was calculated. The findings from the field experiments point to the following:

1. The total strain at the crack induced area varies with time before cracking occurs, so the perfectly restrained boundary condition is not true for epoxy coated steel.
2. The longitudinal steel strains across the transverse cracks were measured, which helps to develop proper boundary conditions across cracks for more accurate modeling of CRCP systems.
3. The concrete strain and steel strain in approximately the same place are very different, so it is unreasonable to assume that the epoxy coated steel is completely bonded with concrete in the analysis of the early-age performance of CRCP.
4. The concrete stress was calculated by multiplying the stress dependent strain by the concrete elastic modulus, and the calculated stress was verified against the comparison between the calculated stress at the instant of cracking and the measured tensile strength.

References

1. American Association of State Highway and Transportation Officials, (1993). Guide for Design of Pavement Structures-1993, AASHTO GDPS-4, American Association of State Highway and Transportation Officials, Washington DC, USA.
2. Transportation Research Board of the National Academies, (2004). Guide for Mechanistic-Empirical Design of New and Rehabilitated Structures, *NCHRP 1-37A*, Transportation Research Board of the National Academies, Washington DC, USA.
3. Johnston, D. P. and Surdahl, R. W., (2007). Influence of Mixture Design and Environmental Factors on Continuously Reinforced Concrete Pavement Cracking, *Transportation Research Record*, No. 2020, pp. 83-88.
4. Johnston, D. P. and Surdahl, R. W., (2006). Effects of Base Type on Modeling Long-term Pavement Performance of Continuously Reinforced Concrete Sections, *Transportation Research Record*, No. 1979, pp. 93-101.
5. Zollinger, D. G., Buch, N., Xin, D., and Soares, J., (1999). Performance of Continuously Reinforced Concrete Pavements: Volume VII: Summary, *FHWA-RD-98-102*, Federal Highway Administration, Georgetown Pike, McLean, Virginia, USA.
6. Cho, Y. H., Dossey, T., and McCullough, B. F., (1997). Early Age Performance of CRCP with Different Types of Aggregate, *Transportation Research Record*, No. 1568, pp. 35-43.
7. Nishizawa, T., Shimeno, S., Komatsubara, A. and Koyanagawa, M., (1998). Study on Thermal Stresses in Continuously Reinforced Concrete Pavement, *Transportation Research Record*, No. 1629, pp. 99-107.
8. Kim, S. M., Won, M. C. and McCullough, B. F., (2000). Three-dimensional Analysis of Continuously Reinforced Concrete Pavements, *Transportation Research Record*, No. 1730, pp. 43-52.
9. Kim, S. M, Won, M. C, and McCullough, B. F., (2003). Mechanistic Modeling of Continuously Reinforced Concrete Pavement, *ACI Structural Journal*, 100(5), pp. 674-682.
10. Khazanovich, L, Selezneva, O. I., Yu, H. T. and Darter, M. I., (2001). Development of Rapid Solution for Prediction of Critical Continuously Reinforced Concrete Pavement Stress, *Transportation Research Record*, No. 1778, pp. 54-72.
11. Cao, D., (2001). Research on Structure of Continuously Reinforced Concrete Pavement, PhD Thesis, Chang'an University, Xi'an, China (in Chinese).
12. Zollinger, D. G., Buch, N., Xin, D., and Soares, J., (1999). Performance of Continuously Reinforced Concrete Pavements, Volume VI: CRC Pavements Design, Construction, and Performance, *FHWA-RD-98-102*, Federal Highway Administration, Georgetown Pike, McLean, Virginia, USA.
13. Kohler, E, and Rosler, J., (2006). Accelerated Pavement Testing of Extended Life Continuously Reinforced Concrete Pavement Section, Final Report, *Transportation Engineering Series No. 141*, Illinois Cooperative Highway and Transportation Series No. 289, University of Illinois, Urbana, IL.
14. Kohler, E. and Roesler, J., (2003). Active Crack Control for Continuously Reinforced Concrete Pavements, *Annual Meeting CD-ROM*, Transportation Research Board, National Research Council, Washington DC, USA.
15. Nam, J. H., Kim, S. M. and Won, M. C., (2006). Measurement and Analysis of Early-age Concrete Strains and Stresses: Continuously Reinforced Concrete Pavement under Environmental Loading, *Transportation Research Record*, No. 1947, pp. 79-90.
16. Kim, S. M., Nelson, P. K., Ruiz, M., Rasmussen R. O. and Turner D., (2003). Early-age Behavior of Concrete Overlays on Continuously Reinforced Concrete Pavements, *Annual Meeting CD-ROM*, Transportation Research Board, National Research Council, Washington DC, USA.
17. Fu, Z., Liu, Q. Q., Niu, K.M., Yu, B., Liang, J.L., Xu, J. J., and Yang, Z.T., (2003). Technical Specification for Construction of Highway Cement Concrete Pavements, *JTG F30-2003*, Research Institute of Highway Ministry of Transport, Beijing, China.
18. Bazant, Z. P., (1988). *Mathematical Modeling of Creep and Shrinkage of Concrete*, John Wiley and Sons, Inc., New York.
19. Glisic, B. and Simon, N., (2000). Monitoring of Concrete at Very Early Age Using Stiff SOFO Sensor, *Cement and Concrete Composites*, Vol. 22, pp. 115-119.